ADVANCED OPTICAL MATERIALS
www.advopticalmat.de

High Efficiency Luminescent Solar Concentrator based on Organo-Metal Halide Perovskite Quantum Dots with Plasmon Enhancement

Benaz Mendewala, Evan T. Vickers, Katerina Nikolaidou, Albert DiBenedetto, William G. Delmas, Jin Z. Zhang, and Sayantani Ghosh**

Organo-metal halide perovskites (OMHPs) are currently one of the most exciting candidates for photovoltaics. However, their impact in other areas related to carrier photogeneration, such as in luminescent solar concentrators (LSCs), has been limited. OMHP thin films have demonstrated encouraging results as LSCs, but for a scalable platform with minimal losses, discrete emitters are preferable. Perovskite quantum dots (PQDs) possess higher photoluminescence quantum yield (PLQY) than their thin film counterparts, and have the added advantage of size tunability, which make them well-suited as LSC active media. However, since PQDs are not amenable to Stokes shift modulation, large-scale samples will suffer from increased self-absorption (SA) losses. In this work, a facile dip-coating approach is established to fabricating large-scale LSCs with $CH_3NH_3PbBr_3$ (methylammonium lead bromide) PQDs by leveraging their plasmonic interactions with gold nanoparticles (AuNPs) to offset SA losses. Optical characterization through emission, lifetime, and spatially resolved photoluminescence measurements provide insight into the effect of plasmon resonance on deposited PQDs, and leveraging this AuNP-PQD coupling, 2.87% efficiency is achieved in a 100 cm^2 LSC with a geometric gain of 50.

1. Introduction

Luminescent solar concentrators (LSCs) were originally introduced more than sixty years ago as cost-effective alternatives to traditional photovoltaic (PV) systems.[1–3] Historically, LSCs employed a polymer or glass substrate doped with fluorophores, which down converted and directed incident sunlight to solar cells attached at the edges.[4–6] Since then, the scopes of both design and application of LSCs have broadened considerably, beyond mere cost consideration. One of the most significant advantages of LSC-enabled solar cells is their ability to utilize both direct and diffuse sunlight, thereby negating the necessity of a tracking mechanism.[7] This allows LSCs to be incorporated into otherwise difficult architectures, such as vertical, or even nonplanar surfaces, making them far better suited as building integrated PVs. Another advantage is the versatility LSCs offer in their choice of appearance, where wavelength-selectivity allows both color and transparency to be varied to suit the requirements of installation, such as in "smart" windows.[8–10]

The active materials in LSCs must possess high photoluminescence quantum yield (PLQY) and broadband absorption.[1,7,11] The most commonly used fluorescent components include organic dyes and semiconductor quantum dots (QDs) such as CdSe/CdS, CdSe/ZnS, PbS, and Si.[1,2,5,6,12–16] The highest power conversion efficiency (PCE) to date is 7%, achieved in a dye-based LSC when it is coupled to GaAs photovoltaic (PV) cells.[17] However, this same LSC, when coupled to Si PV cells, displayed a PCE of 2.9%. Furthermore, it had a small geometric gain factor G. Defined as the ratio of the areas of the PV cells to that of the LSC surface that is facing the sun, $G = A_{LSC}/A_{PV}$, G is a critical metric in characterizing LSC performance. In particular, as the LSC is scaled up and G gets larger, the harder it is to achieve high efficiencies. For example, while optical efficiency η_{opt} in the range of 20–40% has been reported in small LSCs[5,7,16,18] with $G \leq 30$, η_{opt} of large area LSCs with $G \geq 45$ ranges from 1% to 2.6%.[19–21] The biggest hurdle that prevents LSCs from practical implementation is this matter of scalability, which arises from "self-absorption" (SA) losses.[1,7,16] In most materials, the spectral overlap of the absorption and emission bands results in the emitted light being reabsorbed by the material, and barring 100% PLQY, this results in further losses. There are several avenues to mitigating SA. Successful strategies

B. Mendewala, K. Nikolaidou, A. DiBenedetto, W. G. Delmas, Prof. S. Ghosh
Department of Physics
University of California
Merced, CA 95343, USA
E-mail: sghosh@ucmerced.edu
E. T. Vickers, Prof. J. Z. Zhang
Department of Chemistry and Biochemistry
University of California
Santa Cruz, CA 95064, USA
E-mail: Zhang@ucsc.edu
The ORCID identification number(s) for the author(s) of this article can be found under https://doi.org/10.1002/adom.202100754.

DOI: 10.1002/adom.202100754

include material engineering, such as thick shells around QD cores[19,16,22] that suppress reabsorption, and chemical modifications to induce a large spectral separation between absorption and emission bands.[23] The result of such effort has been to increase the PLQY of the fluorescent species (≈50–70%), which has then translated to higher optical efficiencies. The question we investigate here is if a fluorescent candidate had an intrinsically high PLQY (>70%), would that be able to compensate for SA losses without any band-engineering to suppress reabsorption.

Organo-metal halide perovskite quantum dots (PQDs) are obvious candidates to examine for use as active media in LSCs, given their consistently high PLQY. So far, PQD-based LSCs have been nearly entirely limited to all-inorganic Cs-PQDs,[24–28] and attempts to ameliorate the self-absorption (SA) loses arising from spectral overlap of emission and absorption bands have included using mixed-halide inorganic PQDs,[3] tandem LSC with inorganic PQDs and carbon dots (η_{opt} ≈ 3%),[11] dual mode LSCs incorporating $CsPbBr_3$ PQDs with TiO_2 nanocrystals (η_{opt}≈ 1.8%),[24] exciton routing using perovskite nanoplatelets,[27] and rare-earth doped Cs-based perovskite nanoparticles.[29] In this work, we focus on evaluating the viability of using organo-metallic halide PQDs as active materials in LSCs and investigate the possibility of scaling up the devices. These "hybrid" PQDs consistently have high PLQY (>80%),[30] and by leveraging plasmonic interactions between gold nanoparticles (AuNPs) and $CH_3NH_3PbBr_3$ (methylammonium lead bromide) PQDs, we demonstrate that AuNP-PQD coupling induces an atypical positive correlation between PQD emission intensity and charge recombination times, enhancing both. Using a facile dip-coating technique, we design a 100 cm^2 planar LSCs comprising PQDs and AuNPs of optimal size that results in a competitive optical efficiency of 2.87%.

2. Results and Discussions

2.1. Synthesis of Surface Passivated $CH_3NH_3PbBr_3$ PQDs

The $CH_3NH_3PbBr_3$ PQDs used in this study are synthesized following an established method[31] and functionalized with acid/amine combinations of aromatic capping ligands including benzoic acid (BA), benzylamine (BZA), and isopropylbenzylamine (IPBZA). These combinations have proven very successful in passivating both positive and negative surface defects of the PQDs.[32] We focus chiefly on PQDs ligated with BZA-BA, as the PLQY in solution is the highest (≈80%).[31] The average PQD sizes for these samples are 6.3 ± 1.2 nm. The AuNPs used are 5 and 10 nm in diameter (Nanopartz) and functionalized with carboxylic acid.

2.2. Spectral Characterization

Figure 1 compares spectral changes in the PQDs with the addition of AuNPs. Figure 1A shows that the absorption of films of PQDs with 5 nm AuNPs is greater compared to the control sample. The localized surface plasmon resonance (LSPR) of the AuNP extinction spectrum in Figure 1B overlaps nearly perfectly with the excitonic absorption peak of the PQDs. PQD photoluminescence (PL) is also enhanced in the presence of the AuNPs, shown in Figure 1C and the spectral full width at half maximum (FWHM) of the PL is indicated by dashed lines in Figure 1B for reference. A systematic measurement tracking the spectrally-integrated PQD PL in films prepared with varying AuNP concentration in Figure 1D shows that ≈40 ppm of 5 nm AuNPs is optimal for PL enhancement. At this concentration, PLQY is 77%, a 13% increase from PLQY of the control sample. The PL quenching at higher concentrations of AuNPs

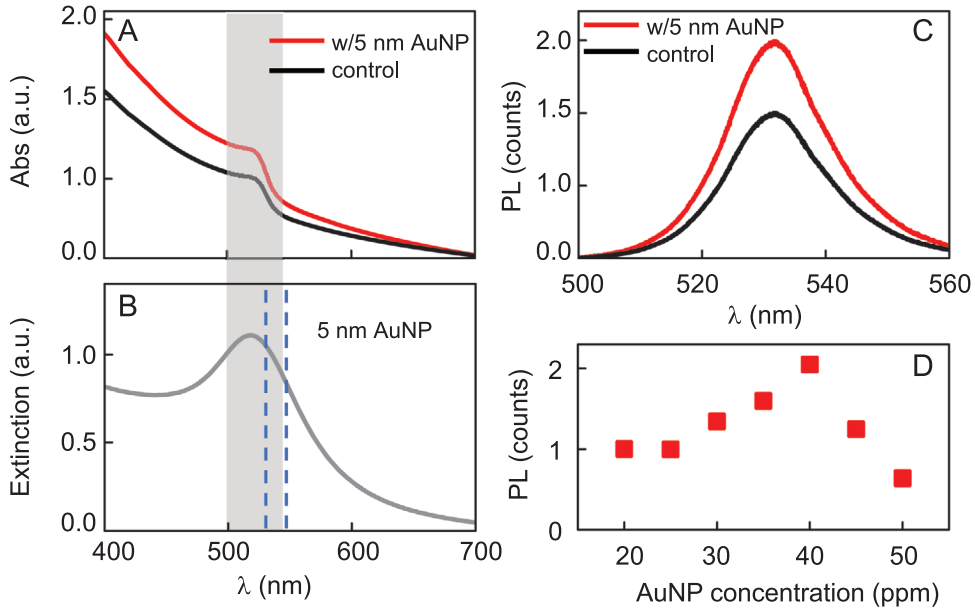

Figure 1. A) Absorption spectra of $CH_3NH_3PbBr_3$ PQDs with and without 5 nm AuNPs. B) Extinction spectrum of 5 nm AuNPs. The gray shaded region highlights the spectral overlap between the PQD excitonic peak and AuNP LSPR. Dashed lines indicate the spectral FWHM of PQD PL. C) PL emission spectra of PQDs with and without the AuNPs. D) Integrated PL intensity varying with 5 nm AuNP concentration.

can be attributed to the decreasing separation between the PQDs and the AuNPs. Exciton plasmon coupling is strongly distance-dependent, and in any ensemble of plasmonic media and fluorophores, there is an optimal separation between the two species for emission enhancement of the latter. For separations shorter than that, energy transfer between them leads to PL quenching. Details of relative concentrations of AuNPs and PQDs, and how these are calculated, are provided in the Supporting Information.

2.3. Time-Resolved Photoluminescence

In addition to changes in static spectral properties, the enhanced electric fields in the vicinity of the plasmonic NPs alter the recombination rates of affected fluorophores, which changes the charge recombination lifetimes. In **Figure 2** we compile spatial maps of integrated PL emission intensity and charge recombination lifetime (measured through time-resolved PL) for drop casted films comprising PQDs alone (control), and PQDs with 5 nm AuNPs. For the PQD-AuNP films we use 40 ppm AuNPs as that showed the largest PL enhancement in Figure 1D. Figure 2A,B plots the PL intensity for the two samples over a 50 × 50 μm^2 area on each film, obtained using scanning PL confocal microscopy. At each spot on the films, we acquire both the PL spectrum and the time-resolved PL data. The latter is then fit to a bi-exponential function $I(t) = A_1 e^{-t/\tau_1} + A_2 e^{-t/\tau_2}$, the average recombination lifetime[33] calculated as $\tau = (A_1\tau_1^2 + A_2\tau_2^2)/(A_1\tau_1 + A_2\tau_2)$, and mapped in Figure 2C,D. The intensity maps confirm the results in Figure 1, where on average 5 nm AuNPs lead to PL enhancement. The τ for the control sample averaged over the mapped region is 9.5 ns and that of the PQDs with 5 nm AuNP is 14 ns.

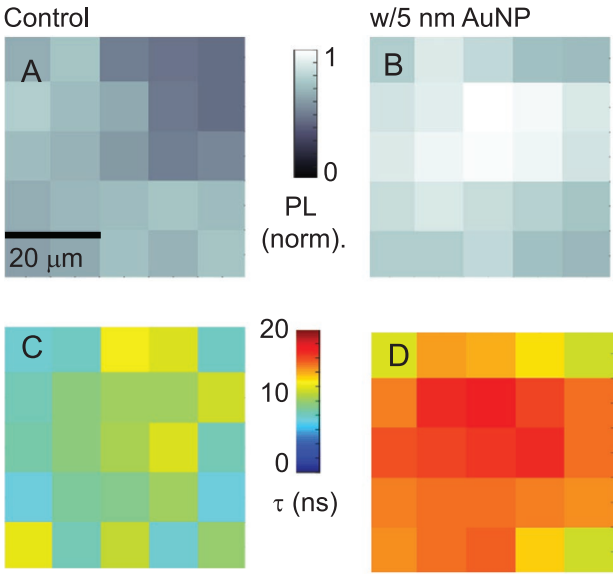

Figure 2. Spatially resolved maps of PL intensity and corresponding recombination lifetime of drop-casted samples. PL intensity of PQD films A) without AuNPs (control) and B) with 5 nm AuNPs over 50 × 50 μm^2 area. Equivalent maps of recombination lifetimes τ for the same, C) without and D) with AuNPs of PQD films.

The increase in PLQY from 68% in the control film to 77% in the PQD-AuNP film would normally indicate radiative energy transfer between the PQDs and the AuNPs. This is usually accompanied by increased radiative recombination driven by the availability of an additional relaxation channel for the photogenerated carriers. In most cases, this leads to the observance of a decreased recombination lifetime. The increased τ of the PQDs with 5 nm AuNPs is, therefore, unexpected. There have been some instances when plasmon-exciton interactions have led to increased recombination lifetime,[34,35] but this is not typical.[36] Further analysis of the data in Figure 2 follows in **Figure 3**. Figure 3A plots the PL counts versus the τ of each point on the maps in Figure 2. The control sample does not show any observable trend, but there is a clear correlation between the intensity and lifetime of the PQD film with 5 nm AuNPs. A linear pairwise correlation analysis returns a coefficient of 0.82, quantifying the atypical increase of charge lifetime with plasmonic emission enhancement. Next, we separate the radiative and non-radiative recombination rates of the PQDs. The PLQY Φ is related to the recombination rates as $\Phi = k_R/(k_R + k_{NR})$ where k_R and k_{NR} are the radiative and nonradiative recombination rates.[37] Using measured values of PLQY and the recombination lifetime from the time-resolved data, we extract both k_R and k_{NR}, plotted as histograms in Figure 3B. What these demonstrate is that the radiative recombination rate does increase with the inclusion of 5 nm AuNPs, which affirms expected plasmonic-excitonic interactions. However, what

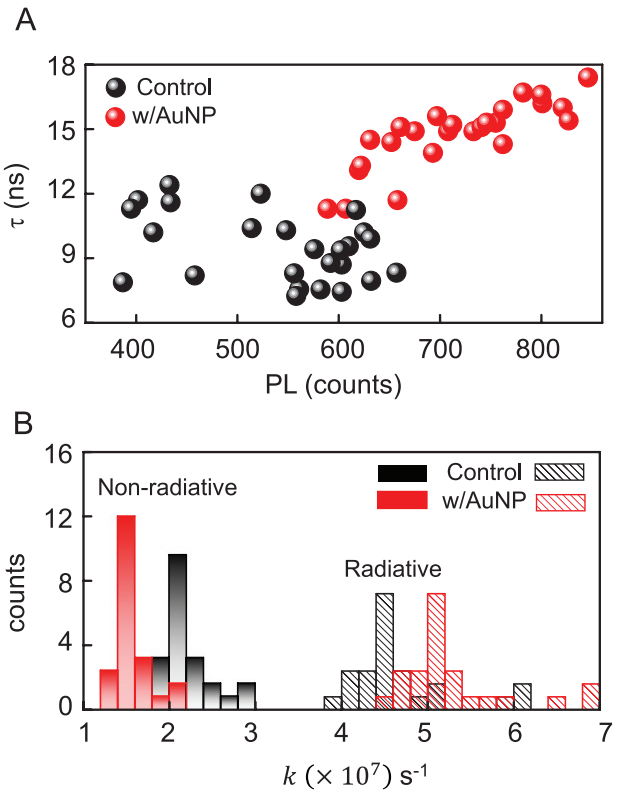

Figure 3. A) Recombination lifetime τ plotted with PL counts for the PQDs without (control) and with 5 nm AuNPs. B) Radiative and nonradiative recombination rates for the two samples.

is more interesting is that the total nonradiative recombination rate decreases in the presence of the AuNPs, which could explain the observed increase of overall charge carrier lifetime.

The suppression of k_{NR} due to addition of AuNPs is unusual, and one possibility is additional PQD surface passivation through interactions with the ligands on the AuNPs. As a check, we repeated all the measurements described in Figures 1 and 2 with 10 nm AuNPs and PQDs. The results show PQD PL quenching as 10 nm AuNP concentration is varied from 20–50 ppm with no enhancement (Figure S1, Supporting Information). Spatially resolved PL and time-resolved PL (Figure S2, Supporting Information) confirm PL quenching and an average lifetime of 8.4 ns, shorter than that of the control sample. These results indicate this is not a passivation effect of the PQDs but related to the LSPR overlap with the excitonic energy. To further verify any atypical issues that may arise from surface-related interactions of the other AuNPs, or from the inherent non-uniformity that may exist in drop-casted films, we investigate the effect of plasmon-exciton coupling on a substrate with patterned gold NPs instead of colloidal ones.

2.4. Patterned Au Substrate

We fabricate patterned Au substrates on p-type silicon (Si) by spin-coating a mixture of poly(styrene-b-2-vinylpyridine) and $HAuCl_4$ in toluene, followed by UV-Ozone treatment at 150 °C for 20 min in O_2 environment to remove the polymer. The resultant AuNPs measure on average 6.5 nm in diameter, with a uniform interparticle spacing of ≈70 nm, shown in the scanning electron microscopy (SEM) image in **Figure 4**A. BZA-BA ligated PQDs films are casted as before, and Figure 4B,C reaffirm all the results observed with the colloidal AuNPs. The PL

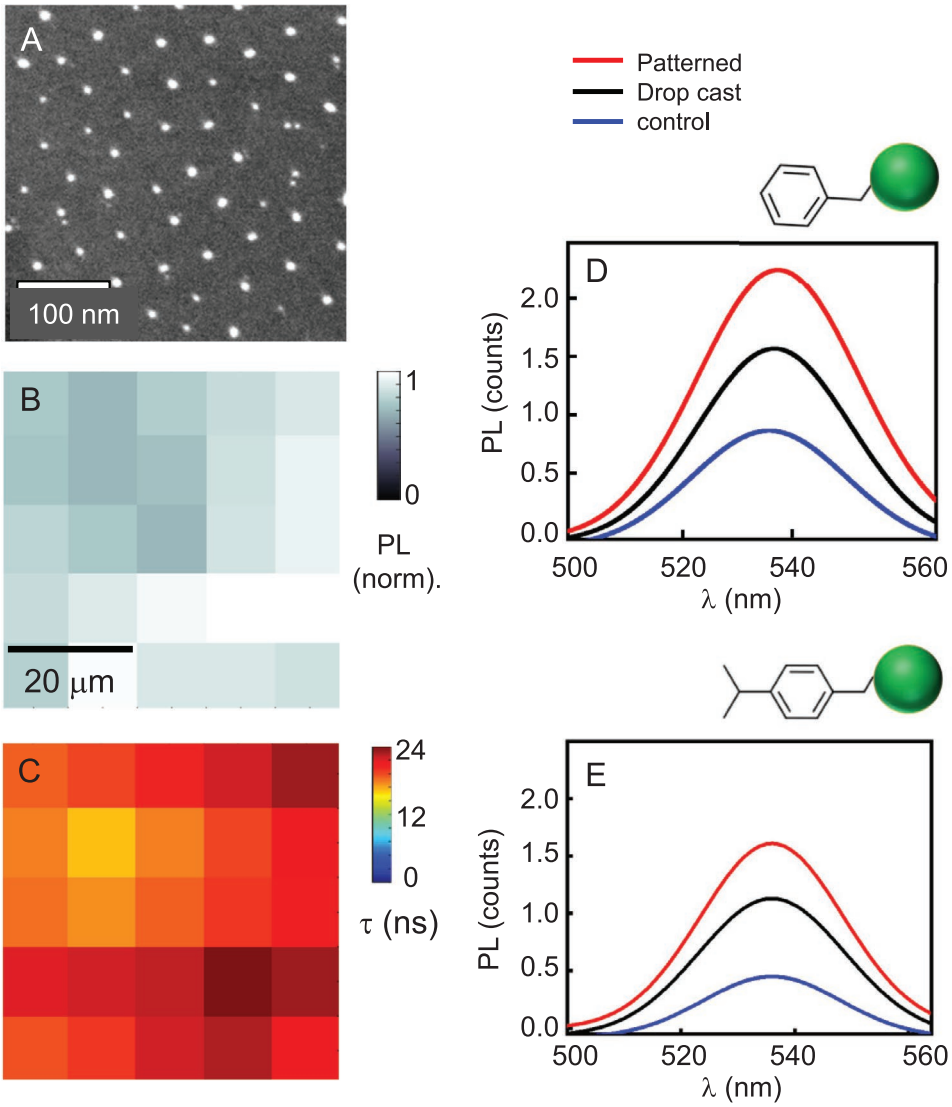

Figure 4. A) SEM image of Au-patterned substrate. Spatially-resolved maps of B) PL emission and C) recombination lifetime τ of PQDs deposited on the Au-pattered Si substrate. PL spectra of PQDs ligated with D) BZA-BA and E) IPBZA-BA, without AuNPs, with 5 nm AuNPs and on Au patterned substrates. Accompanying schematics represent ligand molecular structures and a PQD.

intensity (normalized to counts in Figure 3A for comparison) and recombination lifetime are higher than in the control sample, with the latter averaging 21 ns over the scanned area. It also shows a positive correlation between PL counts and corresponding τ with a coefficient of 0.79. Additional results are shown in Figure 4D,E, where we compare the emission spectra of PQDs ligated with two different ligands, BZA-BA and IPBZA-BA. In both cases we observe the same trend: drop casted AuNP films enhance PQD PL by a factor of two compared to the control and the patterned substrate by nearly a factor of three.

This section verifies that the PL and recombination lifetime enhancements observed are not related to specific ligand–ligand interactions between the PQDs and AuNPs, or to possible interactions between PQDs and substrates. The results do vary with AuNP size as 10 nm AuNPs quench PL and increase the total recombination rate (Figures S1 and S2, Supporting Information). The decrease in the non-radiative recombination rate, highlighted in Figure 3B, that leads to the overall increased recombination lifetimes, is likely still due to improved surface passivation of the PQDs, but driven by LSP-exciton coupling. The strong spectral overlap between PQD absorption and the LSPR peak may allow energy transfer that passivates optically inactive trap states in the former. A similar mechanism has been suggested,[35] and it may also explain why the 10 nm AuNPs do not demonstrate the same effect. The overlap between PQD emission and LSPR is stronger in those, which leads to stronger radiative emission coupling instead. The trap passivation could either take the form of exciting carriers out of the trap states to allow recombination at the band edge, or the form of trap-filling, therefore reducing nonradiative recombination. The exact mechanism is not clear yet, requiring further systematic study, but it is consistent, which leads us to the next step of leveraging it to improve LSC performance.[38–40]

2.5. LSC Design and Efficiency

Although both PQD emission and lifetime demonstrate highest improvement when deposited on the patterned substrate, neither it, nor a drop-casted film, is viable for large scale samples. The former would be expensive, and require inflexible substrates, while the latter has inherent non-uniformity in nanoparticle density. Instead, we employ a simple dip-coating procedure to ensure uniform AuNP and PQD coverage, to create a sample as shown in **Figure 5**A. The samples are synthesized by first preparing a 1.0×10^{-3} M 1,2-ethanedithiol (EDT) in acetonitrile solution. ITO (indium tin oxide) substrates dip-coated with EDT/acetonitrile solution are dipped in the AuNP solution, then slowly lifted out at a rate of ≈1 cm s^{-1}. The samples are then rinsed in pure acetonitrile at the same dipping rate, then rotated 90° to ensure uniformity and the process repeated five times. Once dry, the PQDs are deposited similarly, using the EDT/acetonitrile solution in between PQD layers. We cover the back surface of the substrates with masking tape prior to dip-coating which ensures only one surface is coated. The tape is removed and reapplied after every dip. Once our synthesis procedure was optimized, we successfully produced a small-scale 1.5×1.5 cm^2 (Figure 5B is an edge SEM image of the small-scale LSC showing the final film thickness to be ≈1 μm) and large-scale 10×10 cm^2 LSC by dip-coating the optimal 40 ppm AuNP solution followed by the PQD solution. Our samples consist of AuNP/AuNP/PQD/PQD/AuNP/AuNP/PQD/PQD...layers, with each tetralayer dip-coating repeated for a total of 20 times for the large LSCs. This process, alternating between AuNP and PQD solutions, would create a film ≈500 nm thick. Figure 5C displays a photograph of the large-scale LSC, showing uniform and even coverage with the PQD solution shown adjacently. Figure 5D is the LSC under UV illumination. As a control, an identical 10×10 cm^2 LSC dip-coated with PQDs alone was also synthesized, with approximately the

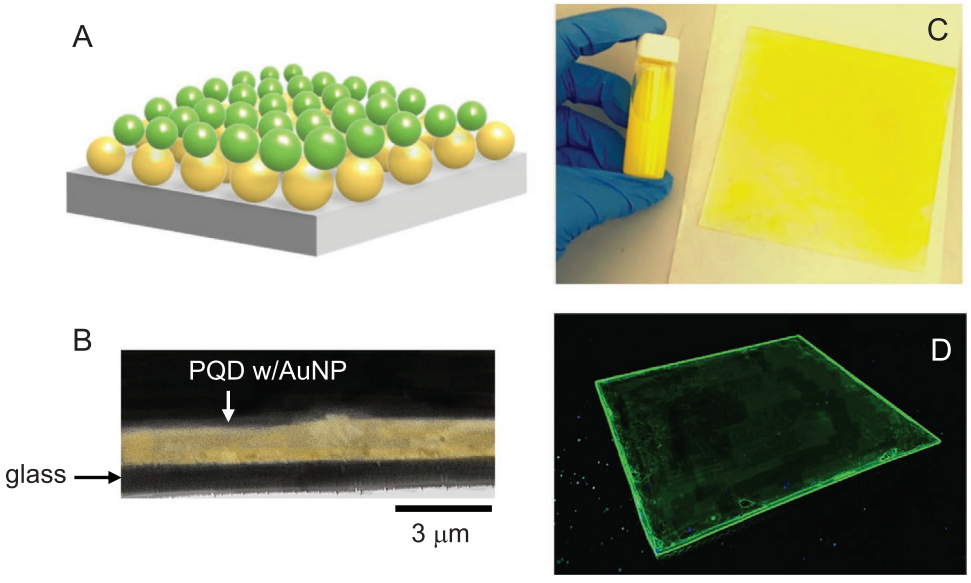

Figure 5. A) Schematic of the PQD-AuNP configuration in the large dip-coated LSC. B) Edge SEM image of large LSC film on glass substrate. Photographs in C) light and D) under UV illumination of the 100 cm^2 LSC.

same number of PQD layers as in the LSC with AuNPs for consistency.

Figure 6A shows the PL enhancement for the 100 cm^2 LSC using a white light source. We observe emission enhancement of 35% relative to the control sample, which is 5% higher than the enhancement shown in Figure 2. With this encouraging result, we assess the performance of both the control and the PQD-AuNP LSC. There are two main loss mechanisms in LSCs. One is through the surface where light incident at angles smaller than the critical angle is not trapped by total internal reflection. The refractive index of OMHP thin films (n = 2.5) is higher than the usual polymer or glass substrates over the range of the solar spectrum. In $CH_3NH_3PbBr_3$ PQDs n varies in this spectral range, averaging ≈2.2. This accounts for a surface trapping efficiency η_{trap} = 89%, significantly higher than the η_{trap} = 75% achieved with n = 1.5 films. The second loss avenue is self-absorption (SA), where the spectral overlap of emission and absorption bands, coupled with PLQY < 100%, lead to reabsorption but not re-emission of the down converted photons. While our PQDs do have substantial spectral overlap, as seen in Figure 1A–D, the high PLQY could potentially offset these loses. We use a well-established pump-probe measurement to estimate the SA.[19,41,42] The sample is mounted on a motorized translation stage with a collection fiber coupled to the sample edge, and a localized excitation spot (focused through a lens and ≈250 µm in diameter) is translated across the LSC surface. However, not all the intensity loss estimated by this approach can be attributed to SA, as there is also scattering-induced loss within a film comprising multilayers of nanoparticles. To separate the contributions from the latter, we follow the procedure outlined in ref. [19], and perform the pump-probe measurement with excitation wavelength of 720 nm. As this is above the absorption peak of the PQDs, this ensures we can calibrate the scattering of light within the LSC film independent of SA, since we are no longer exciting the PQDs, and hence have no emission. In the control sample scattering accounts for almost 6% of loss of intensity, while in the LSC with AuNPs, the loss is slightly higher, at 8% (Figure S3, Supporting Information). Figure 6B plots the PL emission intensity with excitation below the bandgap as a function of the excitation-collection separation d for 10 × 10 cm^2 LSCs, with and without AuNPs. As expected, the emission intensity drops off with increasing pump-probe separation even after correcting for the scattering losses. We confirm that this is due to SA further by tracking the peak emission wavelength λ_{PEAK} as a function of d. A spectral red-shift with increasing d is a well-established consequence of reabsorption and re-emission in an LSC. Each time an absorption event occurs, the re-emitted photon has a lower energy. The extent of red-shift is a measure of number of reabsorption events, and we observe that the presence of AuNPs makes no difference in that (Figure S4, Supporting Information). Both the spectral-shift and the data in Figure 6B demonstrate significant SA losses, in the range of 12–15%. We have also done reflectivity measurements on the LSCs and found those losses to be 1–3%, in keeping with that in typical QD films.[43]

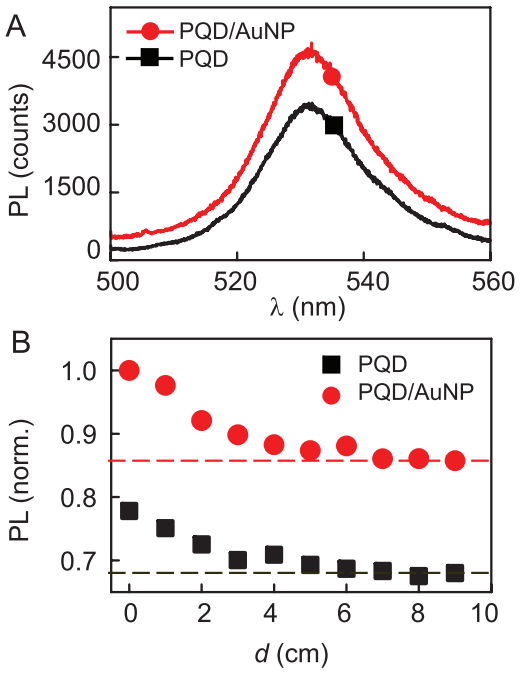

Figure 6. A) PL spectra of 100 cm^2 LSC samples with and without AuNPs. B) Emission intensity in both LSCs as the excitation-to-collection distance d is varied. Dashed lines indicate the maximum loss at largest d.

For optical efficiency measurements, we attach a calibrated Si PV cell along one edge of the LSC with index matched optical gel, while the other three edges are left uncovered. The formula[35] used is $\eta_{opt} = (I_{LSC} \times A_{PV})/(I_{PV} \times A_{LSC})$ where I_{LSC} and I_{PV} are the short-circuit currents generated in the Si PV cell with and without the LSC, and A_{LSC} and A_{PV} are the surface areas of the LSC and the PV cell, in this case measuring 100 and 2 cm^2, respectively. The ratio of the areas, defined as the geometric gain $G = A_{LSC}/A_{PV}$, is 50. All measurements are done in the field under solar illumination under identical conditions, and I_{PV} is measured with sunlight normally incident on the PV. For the control LSC, η_{opt} = 1.72% and for the LSC with PQDs and AuNPs, η_{opt} = 2.87%. Numerically neither of these may seem particularly notable, but to put this in context, we list some comparable η_{opt} and G in **Table 1**. For comparison, our small-scale LSC has a G of 7.5 and corresponding η_{opt} of 68% whereas other low G LSCs show weaker performance.

Finally, we briefly address the issue of stability of performance over time. Methylammonium lead halide perovskite thin films are susceptible to moisture and oxygen, but as we have demonstrated in a previous work,[18] their optical behavior in an LSC is stable at least over a period of weeks under ambient conditions with no encapsulation. A comparative study[24] of LSCs using formamidinium (FA) lead halide PQDs and Cs-PQDs have shown the encouraging results where the former has been stable far longer than the latter. We have monitored PL from both BZA-BA and IPBZA-BA ligated PQDs that were used to investigate the plasmon enhanced emission under continuous illumination with a continuous wave laser at 405 nm. The samples were at 48% relative humidity and at 23 °C (ambient), unencapsulated. We observed significant intensity drop off (Figure S6, Supporting Information) in PQDs ligated with IPBZA-BA, where the intensity decreases by nearly 75% within the first 2 h. BZA-BA PQDs perform moderately better and stabilize at 50% initial intensity after 5 h. The peak

Table 1. Comparison of a selection of recently developed LSCs with $G \geq 45$. Bold text indicates samples from this work.

LSC active material	η_{opt} [%]	G
$CH_3NH_3Br_3$ QDs w/AuNPs	**2.87**	**50**
$CH_3NH_3Br_3$ QDs	**1.72**	**50**
CdSe/CdS QDs[19]	1	43
CdSe/CdPbS QDs[20]	1.15	45
PbS/CdS QDs[21]	1	45
Mixed halide PQDs[3]	2	45
$CsPbX_3$ QDs w/TiO_2[44]	1.82	100

emission energy shift of ≈10 meV in both types of PQDs over this same period is negligible, given the FWHM of the emission is ≈80 meV, indicating no oxidation-induced size changes. Given the large variance in emission stability with the type of ligand used for surface functionalization, this is a route where considerable effort[32,33,45,46] is being invested to improve PQD performance, and by extension, perhaps in their thin film counterparts as well.

3. Conclusion

Perovskite quantum dots were examined as an emergent material for optoelectronic devices. In particular, the role of plasmonic interaction between metallic gold nanoparticles and hybrid PQDs was investigated. Optical characterization through emission, lifetime, and spatially resolved photoluminescence measurements provided insight into the effect of plasmon resonance on deposited PQDs. Examining interactions between PQDs and AuNPs illustrated that PQDs coupled to 5 nm drop-casted AuNPs exhibited 30% emission enhancement and 4 ns lifetime increase relative to PQDs with no AuNPs, while PQDs coupled to substrates patterned with similarly sized AuNPs exhibited 40% emission enhancement and 14 ns lifetime increase. The significant emission enhancement demonstrated by AuNPs when coupled to PQDs suggested that these PQDs could then be excellent LSC candidates. Competitively efficient large-scale LSCs were synthesized via dip-coating, achieving a maximum optical efficiency of 2.87% for 10 cm × 10 cm devices with high quantum yield. Optimization of AuNP concentration allowed for ideal spacing between plasmon and quantum dot, with the highest emission enhancement achieved by 40 ppm AuNP concentration. The addition of 5 nm AuNPs increased PQD emission, absorption and quantum yield without increasing self-absorption significantly.

This work demonstrates the potential of organic-inorganic hybrid perovskites for a range of optical applications, particularly in solar energy, due to their unique optical properties. Building on this work by more deeply examining the role of plasmon resonance and PQD interaction could provide illuminating insight into several nonradiative phenomena. Furthermore, improving on device efficiency, stability and toxicity in PQD and thin film PVSK LSCs could allow hybrid perovskite materials to eventually reach commercial viability as successful solar energy devices.

Supporting Information

Supporting Information is available from the Wiley Online Library or from the author.

Acknowledgements

The authors acknowledge funding from NASA MIRO award no. NNX15AQ01A.

Conflict of Interest

The authors declare no conflict of interest.

Data Availability Statement

Research data are not shared.

Keywords

hybrid perovskites, luminescent solar concentrators, plasmonics, quantum dots, recombination, scalability

Received: April 13, 2021
Revised: June 18, 2021
Published online:

[1] M. G. Debije, P. P. C. Verbunt, *Adv. Energy Mater.* **2012**, *2*, 12
[2] S. Chandra, J. Doran, S. J. McCormack, M. Kennedy, A. Chatten, *Sol. Energy Mater. Sol. Cells* **2012**, *98*, 385.
[3] H. Zhao, Y. Zhou, D. Benetti, D. Ma, F. Rosei, *Nano Energy* **2017**, *37*, 214.
[4] Y. Li, X. Zhang, Y. Zhang, R. Dong, C. K. Luscombe, *J. Polym. Sci., Part A: Polym. Chem.* **2019**, *57*, 201.
[5] S. El-Bashir, F. Barakat, M. AlSalhi, *J. Lumin.* **2013**, *143*, 43.
[6] S. K. E. Hill, R. Connell, J. Held, C. Peterson, L. Francis, M. A. Hillmyer, V. E. Ferry, U. Kortshagen, *ACS Appl. Mater. Interfaces* **2020**, *12*, 4572.
[7] B. Mendewala, K. Nikolaidou, C. Hoffman, S. Sarang, J. Lu, B. Ilan, S. Ghosh, *Sol. Energy* **2019**, *183*, 392.
[8] M. Rafiee, S. Chandra, H. Ahmed, S. J. McCormack, *Opt. Mater.* **2019**, *91*, 212.
[9] I. Papakonstantinou, M. Portnoi, M. G. Debije, *Adv. Energy Mater.* **2020**, *11*, 2002883.
[10] Z. Li, X. Zhao, C. Huang, X. Gong, *J. Mater. Chem. C* **2019**, *7*, 12373.
[11] H. Zhao, D. Benetti, X. Tong, H. Zhang, Y. Zhou, G. Liu, D. Ma, S. Sun, Z. M. Wang, Y. Wang, F. Rosei, *Nano Energy* **2018**, *50*, 756.
[12] C. Lyu, J. Kendall, I. Meazzini, E. Preis, S. Bayseç, U. Scherf, S. Clément, R. C. Evans, *ACS Appl. Polym. Mater.* **2019**, *1*, 3039.
[13] S. K. Nam, K. Kim, J. Kang, J. H. Moon, *Nanoscale* **2020**, *12*, 17265.
[14] D. C. J. Neo, W. P. Goh, H. H. Lau, J. Shanmugam, Y. F. Chen, *ACS Appl. Nano Mater.* **2020**, *3*, 6489.
[15] V. I. Klimov, T. A. Baker, J. Lim, K. A. Velizhanin, H. McDaniel, *ACS Photonics* **2016**, *3*, 1138.
[16] H. Li, K. Wu, J. Lim, H. Song, V. I. Klimov, *Nat. Energy* **2016**, *1*, 16157.
[17] L. H. Slooff, E. E. Bende, A. R. Burgers, T. Budel, M. Pravettoni, R. P. Kenny, E. D. Dunlop, A. Büchtemann, *Phys. Status Solidi RRL* **2008**, *2*, 257.

[18] K. Nikolaidou, S. Sarang, C. Hoffman, B. Mendewala, H. Ishihara, J. Q. Lu, B. Ilan, V. Tung, S. Ghosh, *Adv. Opt. Mater.* **2016**, *4*, 2126.
[19] F. Meinardi, A. Colombo, K. A. Velizhanin, R. Simonutti, M. Lorenzon, L. Beverina, R. Viswanatha, V. I. Klimov, S. Brovelli, *Nat. Photonics* **2014**, *8*, 392.
[20] H. G. Zhao, D. Benetti, L. Jin, Y. F. Zhou, F. Rosei, A. Vomiero, *Small* **2016**, *12*, 5354.
[21] Y. F. Zhou, D. Benetti, Z. Y. Fan, H. G. Zhao, D. L. Ma, A. O. Govorov, A. Vomiero, F. Rosei, *Adv. Energy Mater.* **2016**, *6*, 1501913.
[22] I. Coropceanu, M. G. Bawendi, *Nano Lett.* **2014**, *14*, 4097.
[23] Y. Zhao, R. R. Lunt, *Adv. Energy Mater.* **2013**, *3*, 1143.
[24] J. Tong, J. Luo, L.i Shi, J. Wu, L. Xu, J. Song, P. Wang, H. Li, Z. Deng, *J. Mater. Chem. A* **2019**, *7*, 4872.
[25] Y. Zhou, H. Zhao, D. Ma, F. Rosei, *Chem. Soc. Rev.* **2018**, *47*, 5866.
[26] H. Zhao, R. Sun, Z. Wang, K. Fu, X. Hu, Y. Zhang, *Adv. Funct. Mater.* **2019**, *29*, 1902262.
[27] M. Wei, F. P. G. de Arquer, G. Walters, Z. Yang, L. N. Quan, Y. Kim, R. Sabatini, R. Quintero-Bermudez, L. Gao, J. Z. Fan, F. Fan, A. Gold-Parker, M. F. Toney, E. H. Sargent, *Nat. Energy* **2019**, *4*, 197.
[28] A. K. Singh, *Methods Appl. Fluoresc.* **2020**, *8*, 045008.
[29] T. Cai, J. Wang, W. Li, K. Hills-Kimball, H. Yang, Y. Nagaoka, Y. Yuan, R. Zia, O. Chen, *Adv. Sci.* **2020**, *7*, 2001317.
[30] F. Zhang, H. Zhong, C. Chen, X. Wu, X. Hu, H. Huang, J. Han, B. Zou, Y. Dong, *ACS Nano* **2015**, *9*, 4533.
[31] E. T. Vickers, T. A. Graham, A. H. Chowdhury, B. Bahrami, B. W. Dreskin, S. Lindley, S. B. Naghadeh, Q. Qiao, J. Z. Zhang, *ACS Energy Lett.* **2018**, *3*, 2931.
[32] W. G. Delmas, E. T. Vickers, A. C. DiBenedetto, C. Lum, I. N. Hernandez, J. Z. Zhang, S. Ghosh, *J. Phys. Chem. Lett.* **2020**, *11*, 7886.
[33] S. Bonabi Naghadeh, S. Sarang, A. Brewer, A.'L. Allen, S. Ghosh, J. Zhang, *J. Chem. Phys.* **2019**, *151*, 154705.
[34] N. Zhou, M. Yuan, Y. Gao, D. Li, D. Yang, *ACS Nano* **2016**, *10*, 4154.
[35] E. J. Guidelli, A. P. Ramos, O. Baffa, *Sci. Rep.* **2016**, *6*, 36691.
[36] M. Eichelbaum, K. Rademann, *Adv. Funct. Mater.* **2019**, *19*, 2045.
[37] Z. Shi, Y. Li, S. Li, X. Li, D.i Wu, T. Xu, Y. Tian, Y. Chen, Y. Zhang, B. Zhang, C. Shan, G. Du, *Adv. Funct. Mater.* **2018**, *28*, 1707031.
[38] M. Rafiee, S. Chandra, H. Ahmed, K. Barnham, S. J. McCormack, *Opt. Express* **2021**, *29*, 15031.
[39] S. Chandraa, J. Doran, S. J. McCormack, M. Kennedy, A. J. Chatten, *Sol. Energy Mater. Sol. Cells* **2012**, *98*, 385.
[40] V. Levchenko, *J. Lumin.* **2018**, *193*, 5.
[41] V. Sholin, J. D. Olson, S. A. Carter, *J. Appl. Phys.* **2007**, *101*, 123114.
[42] G. V. Shcherbatyuk, R. H. Inman, C. Wang, R. Winston, S. Ghosh, *Appl. Phys. Lett.* **2010**, *96*, 191901.
[43] B. Xie, Y. Cheng, J. Hao, W. Shu, K. Wang, X. Luo, *Sci. Rep.* **2017**, *7*, 16663.
[44] Q. Lu, S. Zu, H. Shao, G. Huang, S. Xu, Y. Ciu, D. Ban, C. Wang, *Nanotechnology* **2020**, *31*, 455205.
[45] E. Vickers, E. E. Enlow, W. Delmas, A. DiBenedetto, A. Chowdhury, B. Bahrami, B. Dreskin, T. Graham, I. Hernandez, S. Ghosh, Q. Qiao, J. Zhang, *ACS Energy Lett.* **2020**, *5*, 817.
[46] B. Luo, Y.-C. Pu, S. A. Lindley, Y. Yang, L. Lu, Y. Li, X. Li, J. Z. Zhang, *Angew. Chem., Int. Ed.* **2016**, *55*, 8864.